Wireless Personal Communications **1**: 271–285, 1995.

Trellis-Coded CPFSK and Soft-Decision Feedback Equalization for Micro-Cellular Wireless Applications

W. Zhuang[1],* W. A. Krzymien[2] ** † & P. A. Goud[2] **

[1] *Department of Electrical and Computer Engineering, University of Waterloo, Waterloo, Ontario, Canada N2L 3G1 (Tel.: 519-885-1211, ext. 5354; Fax: 519-746-3077; E-mail: wzhuang@bbcr.uwaterloo.ca)*

[2] *Telecommunications Research Laboratories, 800 Park Plaza, 10611-98 Avenue, Edmonton, Alberta, Canada T5K 2P7 (Tel.: 403-441-3811; Fax: 403-441-3600; E-mail: wak@trlabs.ca and Department of Electrical Engineering, University of Alberta, Edmonton, Alberta, Canada T6G 2G7; † author for correspondence)*

Abstract

In this paper, trellis-coded M-ary CPFSK with noncoherent envelope detection and adaptive channel equalization are investigated to improve the bit error rate (BER) performance of microcellular digital wireless communications systems. For the same spectral efficiency, the trellis-coded modulation (TCM) schemes studied outperform minimum shift keying (MSK) with noncoherent or differentially coherent detection in Rayleigh fading channels. For the case of frequency-selective fading channels, adaptive channel equalization is applied to mitigate the time-variant intersymbol interference (ISI). A new equalizer structure is proposed which, in its feedback path, makes use of fractionally spaced signal samples instead of symbol-spaced hard decisions on transmitted symbols. Computer simulation results indicate that the soft-decision feedback equalizer (SDFE) can significantly improve the system's performance.

1. Introduction

Continuous-phase modulation (CPM) is an attractive modulation scheme for digital transmission on mobile and indoor radio channels. It has been selected for the second-generation European digital cellular system, i.e., the Group Speciale Mobile (GSM) [1], as well as the Digital European Cordless Telecommunications (DECT) system [2]. The advantages of CPM include: (i) a constant RF envelope, permitting the use of power-efficient nonlinear amplifiers without causing undue nonlinear distortion of the transmitted signal; (ii) a relatively high bandwidth efficiency and low out-of-band power. Trellis-coded continuous-phase frequency shift keying (CPFSK) has been investigated in order to achieve either an even higher spectral efficiency, or else a better transmission performance than its uncoded counterpart MSK (minimum shift keying). Anderson *et al.* [3] and Ho *et al.* [4] have presented a comparison between different classes of trellis-coded CPM schemes with optimal coherent demodulation in an AWGN channel and have investigated design rules for good trellis codes with CPM for the same channel. They have shown that, with an optimal coherent receiver, some trellis-coded modulation (TCM) schemes can achieve either a doubled spectral efficiency or a 5.0 dB asymptotic gain in bit error rate (BER) performance, compared with coherent MSK. The performance improvement of the encoded systems is at the expense of increased receiver complexity: they require a large number of coherent matched filters, and a Viterbi decoder with up to hundreds of states. Furthermore, in mobile and indoor radio channels, coherent detection receivers suffer severely from carrier phase jitter due to rapidly changing channel conditions, so that the comparatively long acquisition time of carrier and clock recovery circuits results in high error floors [5]. Consequently, noncoherent detection of coded CPFSK signals has attracted considerable attention due to its lower circuit complexity, fast synchronization and robustness under fading [6, 7].

* Member IEEE

** Senior Member IEEE

It has been shown that the DECT system with uncoded GMSK (Gaussian filtered minimum shift keying) fails to provide satisfactory bit error rate (BER) performance, i.e. BER $\leq 10^{-3}$, for reliable digital voice transmission in an indoor radio channel when the channel delay spread is relatively large [8]. Diversity reception has been studied for achieving better performance. However, in the case of a large delay spread, the system with diversity can provide only marginal performance at best. Therefore, other channel impairment mitigation techniques are necessary to combat system performance degradation. In this paper, trellis-coded CPFSK with noncoherent detection and adaptive channel equalization are investigated as two techniques for better performance.

The intersymbol interference (ISI) due to multipath propagation in an indoor radio channel is one of the dominant disturbance factors in a high bit rate time-division multiple access (TDMA) system. This interference can be reduced considerably by the proper application of adaptive channel equalization techniques. Conventional decision-feedback equalization techniques are less effective in the system considered here, due to its characteristics of: (i) nonlinearity introduced by both nonlinear modulation and envelope detection, and (ii) the channel delay spread smaller than a symbol duration. A new adaptive channel equalizer structure is proposed which, in the feedback path, makes use of fractionally spaced signal samples instead of symbol-spaced hard decisions on transmitted data, as in a conventional decision feedback equalizer (DFE). The soft-decision feedback equalizer (SDFE) can significantly reduce BER floors of the system studied here.

This paper is organized as follows: The system model (including transceiver structures and indoor fading channels) is described in Section 2. The structure of the newly proposed SDFE is discussed in Section 3. In Section 4, the performance improvement achieved by TCM and by channel equalization over indoor wireless channels is investigated through computer simulations. Conclusions are presented in Section 5.

2. System Model

2.1. Transceiver

The trellis-coded M-ary CPFSK system model is illustrated in Fig. 1. The transmitter consists of a data source, a serial to parallel converter, a rate k/n trellis encoder, an M-level natural mapper, a CPFSK modulator and a frequency up converter for RF transmission. The data source generates an independent and identically distributed (i.i.d.) binary sequence which is converted into a sequence of independent k-bit information words: $\mathbf{a}_i^k = \{a_i^1, a_i^2, ..., a_i^k\}$. The output of the encoder is a sequence of coded n-bit words: $\mathbf{b}_i^n = \{b_i^1, b_i^2, ..., b_i^n\}$, where $b_i^l \in \{0, 1\}$. The natural mapper outputs one of the $M = 2^n$ possible output symbol values according to the following mapping rule:

$$C_i = \sum_{l=1}^{n} b_i^l 2^{n+1-l} - M + 1, \quad i = 1, 2, ..., M. \quad (1)$$

The symbols b_i^1 and b_i^n are referred to as the most significant bit (MSB) and the least significant bit (LSB), respectively. C_i is then used to choose the signal frequency transmitted over $t \in [iT, (i+1)T]$:

$$f_i = f_c + C_i f_d = f_c + \frac{C_i h}{2T}, \quad (2)$$

where f_c is the RF carrier frequency, f_d is the frequency deviation, h is the modulation index and T is the symbol duration. The complex bandpass representation $\tilde{s}_i(t)$ of the RF transmitted signal over $t \in [iT, (i+1)T]$ can be expressed as:

$$\tilde{s}_i(t) = A \exp\{j[2\pi C_i f_d (t - iT) + \theta_i]\} \exp[j2\pi f_c t], \quad (3)$$

where θ_i is the carrier phase at $t = iT$.

The basic modules contained in the receiver are the soft-decision feedback equalizer (SDFE), a soft-decision noncoherent demodulator and a Viterbi decoder. The receiver has the knowledge of all possible frequencies of the transmitted signal, but has no information about the carrier phase. In the demodulator, noncoherent detection is performed over all the possible frequencies. The necessary M decision variables for each symbol interval are evaluated in M parallel branches, each containing noncoherent in-phase (I) and quadrature (Q) correlators followed by an evelope detector, as shown in Fig. 2. In order to achieve the gain of TCM, no hard decision is made at the output of the demodulator. All the envelope detector outputs are used in the Viterbi decoder for soft-decision estimation of the original transmitted information sequence "**a**". Details of the SDFE are discussed in Section 3.

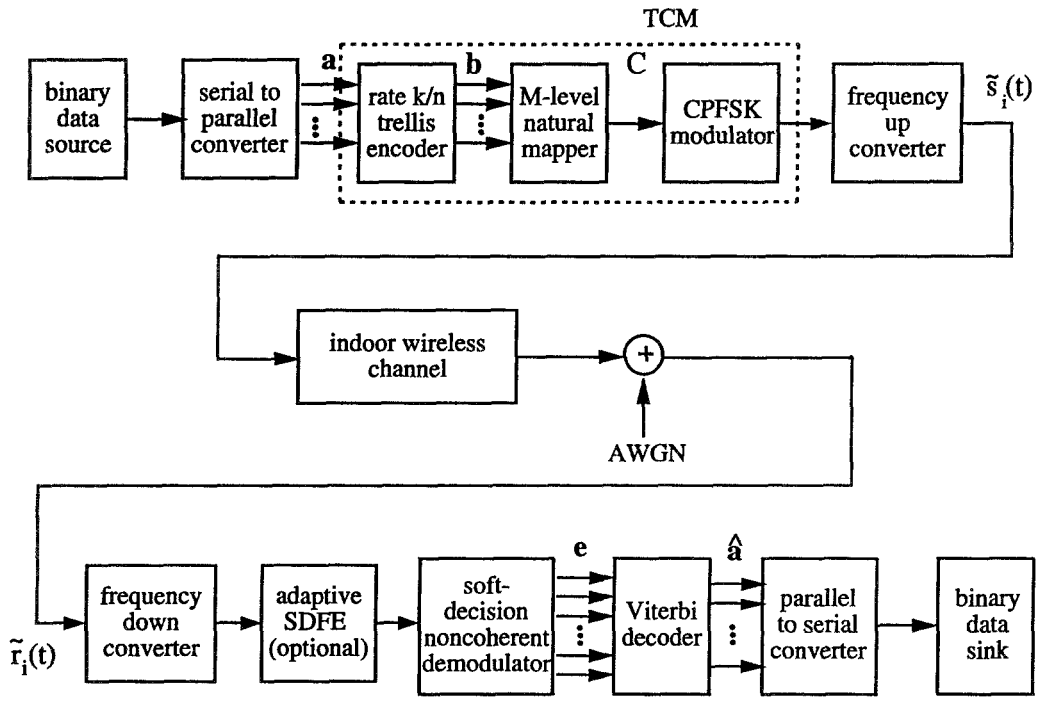

Fig. 1. Functional block diagram of the trellis-coded CPFSK system model.

2.2. *Indoor Radio Channel Model*

The received signal $\tilde{r}_i(t)$ is assumed to be corrupted by a time-variant multipath radio channel with impulse response $\tilde{h}_c(t,\tau)$ and by additive white Gaussian noise (AWGN) $\tilde{n}(t)$ described by one-sided spectral density N_0. In general, the complex baseband channel impulse response can be represented as [9]

$$h_c(t,\tau) = \sum_{l=1}^{L(\tau)} a_l(t)\exp[j\varphi_l(t)]\delta[\tau - \tau_l(t)], \quad (4)$$

where t is the system time, τ is the instant of application of the input impulse, $L(\tau)$ is the number of paths taken into account and τ_l is the propagation delay of the l-th path. Existing indoor radio channel measurements indicate that, for the l-th path, the amplitude distortion $a_l(t)$ is a Rayleigh distributed random process, the carrier phase disturbance $\varphi_l(t)$ is a random process uniformly distributed over $[0, 2\pi]$ and the signal propagation delays $\tau_l(t)$ form a Poisson point process [9, 10]. The power spectral density of $a_l(t)$ is given by the classical Doppler spectrum formula

$$S_l(f) = \begin{cases} P_l/[\pi f_D\sqrt{1-(f/f_D)^2}], & |f| \le f_D \\ 0, & |f| > f_D \end{cases} \quad (5)$$

where P_l is the average received power for the l-th path, and f_D is the maximum Doppler frequency shift. The fading channel is also characterized by its root-mean-square (RMS) delay spread, σ, defined as

$$\sigma = \sqrt{\frac{M_2}{M_0} - \left(\frac{M_1}{M_0}\right)^2}, \quad (6)$$

where

$$M_0 = \int_0^\infty P(t)dt, \quad M_1 = \int_0^\infty tP(t)dt, \text{ and}$$
$$M_2 = \int_0^\infty t^2P(t)dt;$$

$P(t)$ is the power delay profile for a given τ. The channel delay spread can be sufficiently large to cause severe intersymbol interference in a high bit rate TDMA system. At a given τ, the equivalent baseband waveform $r_i(t)$ of the received signal is

$$r_i(t) = s_i(t) \otimes h_c(t,\tau) + n(t). \quad (7)$$

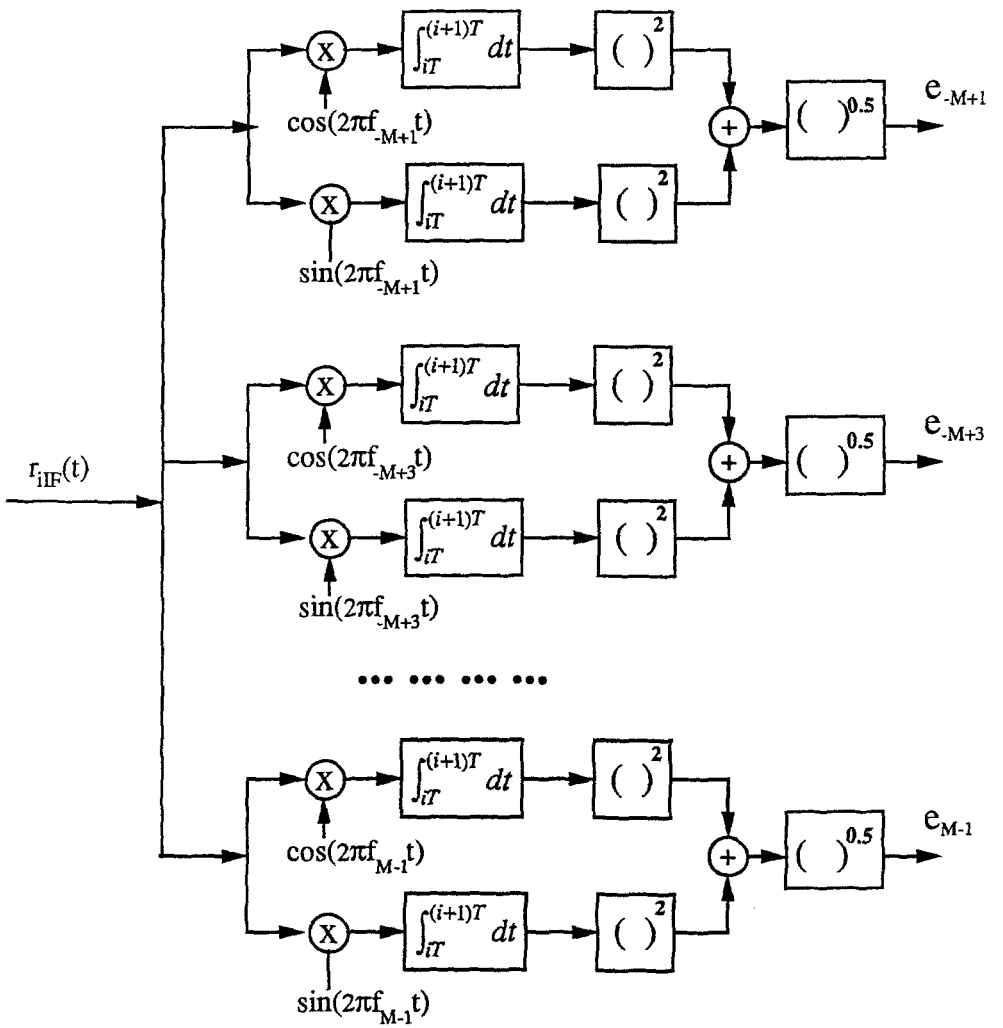

Fig. 2. Soft-decision noncoherent demodulator.

In general, the value of f_DT determines the signal fading rate. When $f_DT \ll 1.0$, the channel exhibits slow fading. For example, in the DECT system, f_D is a few Hz and T is less than one microsecond, so that f_DT is of the order of 10^{-6}. For such a slowly fading channel, it would take a large amount of computer time to obtain an accurate estimate of the BER performance. Therefore, in the following computer simulations, the value of f_DT is chosen in the neighborhood of 0.005, which still characterizes a slowly fading channel.

A six-path Rayleigh fading channel model with exponential power delay profile is used [8]. The classical Doppler spectral spread of each of the paths in this profile is generated using the simulation method described in [11]. This model reasonably represents radio propagation in and around buildings at and around 1.9 GHz (proposed for the DECT system). The typical RMS delay spread for indoor, indoor to outdoor and outdoor environments ranges from 50 to 250 ns, corresponding to approximately $(0.05 \sim 0.25) \cdot T_b$ (where T_b is one bit duration) for the DECT system; that is, the RMS delay spread is smaller than one symbol duration. Table 1 gives three power delay profiles of the indoor channel model, which are used in computer simulations to be discussed later. The first and second profiles are single exponential, and the third is double exponential. Taking into account the amplitude distortion, carrier phase disturbance introduced

Table 1. Power delay profiles of the indoor channel ($\Sigma P_l = 1.0$).

τ/T_b	profile 1: P_l ($\sigma/T_b = 0.125$)	profile 2: P_l ($\sigma/T_b = 0.163$)	profile 3: P_l ($\sigma/T_b = 0.250$)
0.000	0.6000	0.3526	0.3452
0.125	0.2388	0.2497	0.2178
0.250	0.0954	0.1576	0.1543
0.375	0.0426	0.1114	0.0973
0.500	0.0168	0.0790	0.1729
0.625	0.0066	0.0497	0.0000
1.250	0.0000	0.0000	0.0124

by the fading channel, and the fact that the noncoherent demodulator integrates the product of the received signal and the local oscillator waveform over the whole symbol interval, the resultant ISI can degrade the system performance severely.

3. Soft-Decision Feedback Equalizer

Frequency-selective fading of the indoor radio channel introduces linear distortion to both the amplitude and carrier phase of the received RF signal, as mentioned in Section 2. Although the amplitude variations can be removed by amplitude control units, the phase disturbance will result in nonlinear distortion after the nonlinear demodulation. The ISI components at the demodulator output are generated nonlinearly due to the envelope detectors. If equalization is performed at baseband after the demodulator, then the corresponding nonlinear components of the transmitted signal should be introduced to the equalizer for canceling the ISI. If the number of distinct paths in the time-varying channel is larger than two, then it will be very difficult to remove the nonlinear ISI (if not impossible). Another way to equalize the fading channel is to implement the equalization function at passband before the nonlinear demodulator. In this case, the equalizer needs to combat the linear ISI caused only by the fading channel. It is well known that a DFE is more effective than a linear equalizer in combating ISI in the presence of moderate to severe amplitude distortion (e.g., in the case of indoor radio channels) [12, 13]. Decision feedback equalization uses previously detected symbols to synthesize the postcursors of the discrete impulse response that are subsequently subtracted from the received samples through a feedback loop. However, conventional symbol-spaced decision feedback equalization is not effective in mitigating the ISI in this case, because of (i) the nonlinearity of the link introduced by the nonlinear modulator and noncoherent demodulator, and (ii) the RMS delay spread being smaller than a symbol duration. In the following, a new adaptive channel equalizer structure is proposed, which can significantly improve the system performance.

3.1. Post-estimation of the Carrier Phase for Passband Equalization

Passband equalization requires information on the initial carrier phase of the currently received symbol, which is not directly available with noncoherent detection. In the case of a slowly fading channel, the channel impulse response is approximately time-invariant over a m-symbol interval if $(f_D m T) \ll 1.0$. The parameters of an adaptive equalizer obtained from the signals received m-symbol intervals earlier can therefore be used to equalize the currently received signal. The initial carrier phase of the previously received symbols can be obtained after the symbols have been correctly detected (or decoded). As a result, passband channel equalization becomes possible for slowly fading channels. With the noncoherent envelope detector, the carrier phase can be estimated from the correlator outputs of the in-phase (I) and quadrature (Q) paths, and from the detected transmitted symbols. For simplicity, no ISI and input noise are considered in the following derivation. The equivalent passband (IF) waveform of the received CPFSK signal is

$$r_{iIF}(t) = A_{1i}\cos[\omega_{IF}t + 2\pi C_i f_d(t - iT) + \psi_i], \quad t \in [iT, (i+1)T] \tag{8}$$

where ω_{IF} is the IF radian frequency, $A_{1i} = Aa_{1i}$ is the amplitude of the signal, taking account of the amplitude Rayleigh fading of the first path $a_{1i} = a_1(t)$, $t \in [iT, (i+1)T]$, and $\psi_i = \theta_i + \varphi_{1i}$ is the initial carrier phase of the i-th symbol (to be estimated) taking account of the carrier phase disturbance $\varphi_{1i} = \varphi_1(t)$, $t \in [iT, (i+1)T]$, introduced by the fading channel. The signal generated by the jth receiver in-phase local oscillator (Fig. 2) is

$$l_{Ij}(t) = \cos[\omega_{IF}t + 2\pi C_j f_d(t - iT) + \alpha_j], \tag{9}$$

where α_j is the carrier phase of the oscillator at $t = iT$, $C_j f_d$ is the frequency offset of the oscillator over $t \in [iT, (i+1)T]$. The output of the jth in-phase correlator

is then

$$\begin{aligned} e_{Ij} &= \int_{iT}^{iT+T} r_{iIF}(t) l_{Ij}(t) dt \\ &= (A_{1i}T/2)\text{sinc}[(C_i - C_j) f_d T] \\ &\quad \cos[(C_i - C_j)\pi f_d T + \psi_i - \alpha_j]. \end{aligned} \quad (10)$$

The signal generated by the jth receiver quadrature local oscillator is

$$l_{Qj}(t) = \sin[\omega_{IF} t + 2\pi C_j f_d (t - iT) + \alpha_j], \quad (11)$$

and the output of the jth quadrature correlator is

$$\begin{aligned} e_{Qj} &= \int_{iT}^{iT+T} r_{iIF}(t) l_{Qj}(t) dt \\ &= -(A_{1i}T/2)\text{sinc}[(C_i - C_j) f_d T] \\ &\quad \sin[(C_i - C_j)\pi f_d T + \psi_i - \alpha_j]. \end{aligned} \quad (12)$$

Let

$$\begin{aligned} \phi_j &= \arctan[-e_{Qj}/e_{Ij}] \\ &= (C_i - C_j)\pi f_d T + \psi_i - \alpha_j, \end{aligned} \quad (13)$$

then

$$\begin{aligned} \phi &= \sum_{j=1}^{M} \phi_j \\ &= M C_i \pi f_d T + M\psi_i - \sum_{j=1}^{M} (C_j \pi f_d T + \alpha_j) \\ &= M[C_i \pi f_d T + \psi_i]. \end{aligned} \quad (14)$$

In deriving (14), the fact that $\sum_{j=1}^{M} C_j = 0$ and $\sum_{j=1}^{M} \alpha_j = 2n\pi$ (n is an integer) has been taken into account; the latter is the case when all the receiver local oscillator signals are generated from one master oscillator in a frequency synthesizer. From (14) and the detected symbol $\hat{C}_i$, an estimate of the carrier phase can be obtained

$$\hat{\psi}_i = \frac{1}{M} \left\{ \sum_{j=1}^{M} \arctan[-e_{Qj}/e_{Ij}] - M\hat{C}_i \pi f_d T \right\}. \quad (15)$$

It should be pointed out that: (i) the carrier phase estimate will have an error component due to the signal component with frequency $2\omega_{IF}$ at the output of the correlators; (ii) there may exist phase ambiguity of $(2n\pi)/M$ due to the phase averaging operation of (15), which can be detected and removed. Due to the existence of residual intersymbol interference and input noise, the carrier phase estimate will unavoidably contain some error, which is negligible in the case of the input signal having a high E_b/N_0 value.

3.2. *The Receiver Structure with SDFE*

Figure 3 shows a more detailed receiver functional block diagram at passband and baseband. For TCM schemes, the decision device contains a Viterbi decoder and a parallel-to-serial converter. If the decoding depth of the Viterbi decoder is m, then the decision device introduces a time delay of mT ($= mNT_s$), where N is the number of samples in each symbol interval and T_s is the sampling interval. The carrier phase estimator takes the input signals from the noncoherent demodulator and the natural mapper, and estimates the initial carrier phase $\hat{\psi}_{i-m} = \hat{\theta}_{i-m} + \hat{\varphi}_{1(i-m)}$ of the $(i-m)$th symbol according to (13)–(15). The trellis encoder and the natural mapper generate the estimated symbol $\hat{C}_{i-m}$ based on the decision variable $\hat{\mathbf{a}}_{i-m}^{k}$. With $\hat{C}_{i-m}$ and $\hat{\psi}_{i-m}$, the baseband CPFSK modulator (baseband representation of a CPFSK modulator) regenerates an estimated complex baseband signal of the $(i-m)$th symbol as

$$\begin{aligned} &\hat{s}_i(t - mT) \\ &= \exp[2\pi \hat{C}_{i-m} f_d (t - iT - mT) \\ &\quad + \hat{\psi}_{i-m}], \quad t \in [iT, (i+1)T]. \end{aligned} \quad (16)$$

The received passband signal is delayed by mT and converted into a complex equivalent baseband signal by the baseband signal extractor, which for a given τ can be represented as

$$\begin{aligned} &r_i(t - mT) \\ &= s_i(t - mT) \otimes h_c(t - mT, \tau) + n(t - mT), \\ &\quad t \in [iT, iT + T]. \end{aligned} \quad (17)$$

The detailed structure of the baseband SDFE is given in Fig. 4. The delays for the digital shift registers of the feed-forward and feedback transversal filters are $\beta_1 T_s \leq T$ (with M_1 taps) and $\beta_2 T_s \leq T$ (with M_2 taps) respectively, where β_1 and β_2 are integers. The essential difference between a conventional DFE and SDFE is that the feedback signal of the SDFE contains multiple samples of the regenerated CPFSK signal in each symbol interval; therefore, the feedback filter of the SDFE is fractionally spaced which results in effective equalization for delay spreads smaller than one symbol interval. In this way, the SDFE can combat the ISI effectively. The recursive least-squares (RLS)

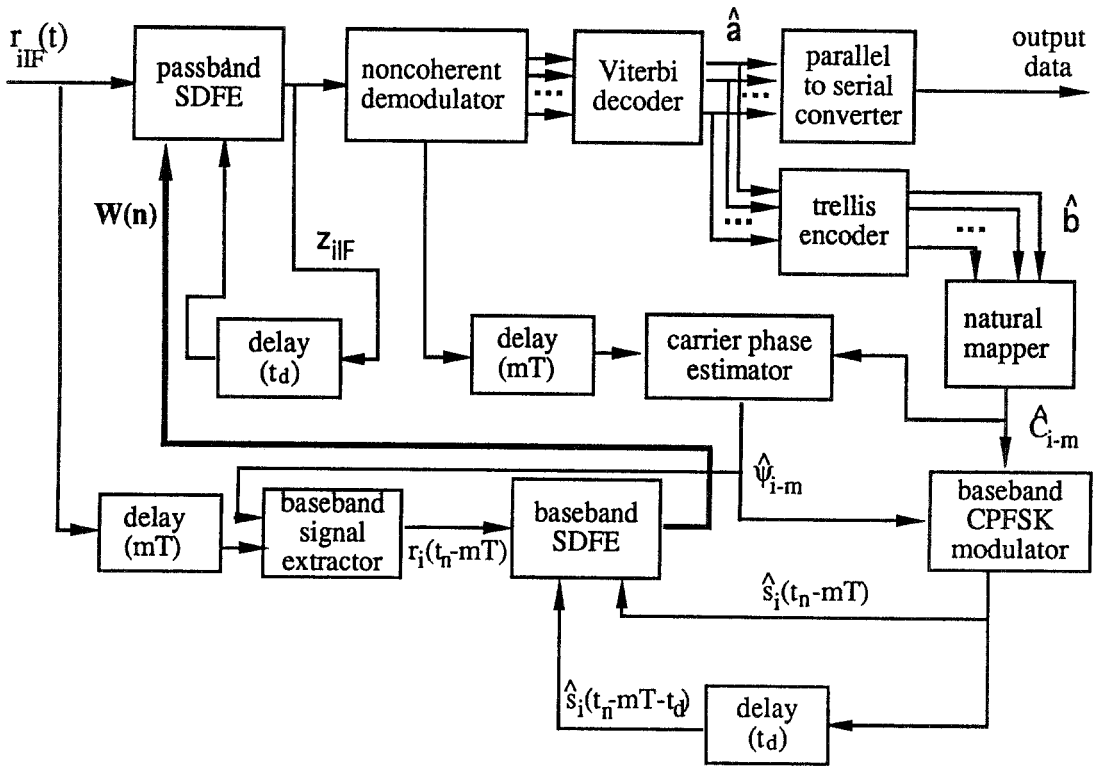

Fig. 3. Receiver structure with SDFE.

algorithm is used in the equalizer due to its fast convergence when compared with the least-mean-square (LMS) algorithm [14]. The RLS algorithm operates on the following input signals: the discrete received baseband signal

$$\begin{aligned}\mathbf{r}(n) &= \mathbf{r}_i(t_n - mT)|_{t_n=n\beta T_s} \\ &= \{r_i(t_n - mT), r_i(t_n - mT - \beta_1 T_s), ..., \\ &\quad r_i(t_n - mT - M_1\beta_1 T_s)\}|_{t_n=n\beta T_s}, \quad (18)\end{aligned}$$

where $t_n \in [iT, iT+T]$, n is an integer, and $\beta = \min\{\beta_1, \beta_2\}$; the soft-decision feedback signal

$$\begin{aligned}\hat{\mathbf{s}}(n) &= \hat{\mathbf{s}}_i(t_n - mT - t_d)|_{t_n=n\beta T_s} \quad (19) \\ &= \{\hat{s}_i(t_n - mT - t_d), \hat{s}_i(t_n - mT - \beta_2 T_s - t_d) \\ &\quad , ..., \hat{s}_i(t_n - mT - M_2\beta_2 T_s - t_d)\}|_{t_n=n\beta T_s},\end{aligned}$$

where $t_d = DT_s \leq T$ is the time delay of the decision feedback signal (D is an integer), and the corresponding innovation is

$$\begin{aligned}\hat{\varepsilon}(n) &= \hat{\varepsilon}_i(t_n - mT) \\ &= \hat{s}_i(t_n - mT) - y_i(t_n - mT)|_{t_n=n\beta T_s} (20)\end{aligned}$$

where

$$\begin{aligned}&y_i(t_n - mT)|_{t_n=n\beta T_s} \\ &\sum_{j=0}^{M_1} c_j(n) r_i(t_n - mT - j\beta_1 T_s)\Big|_{t_n=n\beta T_s}, \\ &- \sum_{j=1}^{M_2} d_j(n)\hat{s}_i(t_n - mT - t_d - j\beta_2 T_s)\Big|_{t_n=n\beta T_s} \quad (21)\end{aligned}$$

is the output of the equalizer with $\mathbf{c}(n) = \{c_0(n), c_1(n), ..., c_{M_1}(n)\}$ and $\mathbf{d}(n) = \{d_1(n), d_2(n), ..., d_{M_2}(n)\}$ being the previously calculated equalizer complex coefficients for the feed-forward and feedback transversal filters, respectively. The complex tap coefficients are set to provide both amplitude and carrier phase compensation. The RLS algorithm optimizes the coefficients of the two filters under a criterion of minimizing the exponentially weighted squared error at time $t_{n+1} = t_n + \beta T_s$, namely

$$J(n+1) = \sum_{l=0}^{n+1} \lambda^{(n+1)-l} [\hat{s}_i(t_l - mT)$$

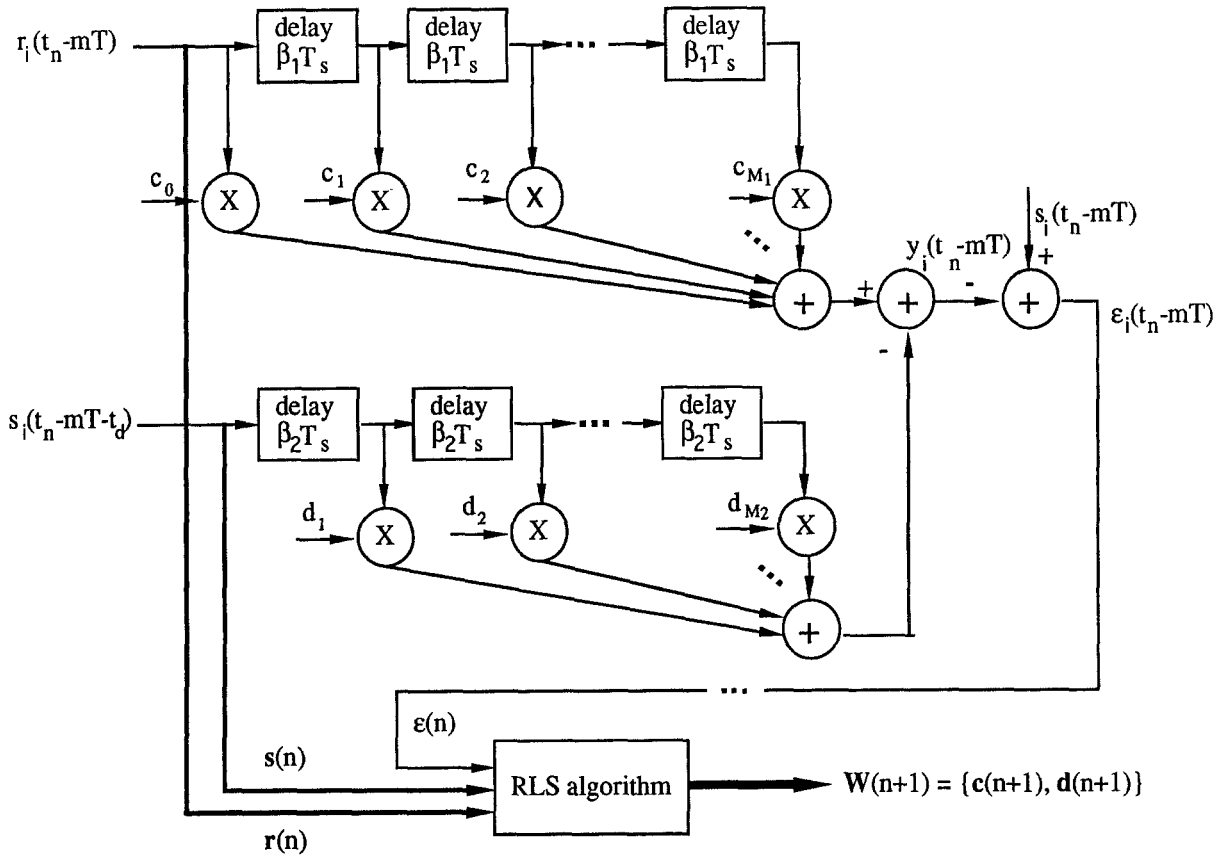

Fig. 4. Baseband SDFE.

$$- \mathbf{r}^*(l)\mathbf{c}^T(l) + \mathbf{s}^*(l)\mathbf{d}^T(l)]^2\big|_{t_l = l\beta T_s}, \quad (22)$$

where the superscripts * and ^{T} indicate complex conjugation and transposition, respectively, and λ is a positive number close to, but less than 1.0 in order for the SDFE to track the variations of the channel impulse response with time. The RLS algorithm calculates the complex equalizer coefficients $\mathbf{w}(n+1) = \{\mathbf{c}(n+1), \mathbf{d}(n+1)\}$ recursively as

$$\mathbf{w}(n+1) = \mathbf{w}(n) + \mathbf{k}(n+1)\hat{\varepsilon}^*(n+1), \quad (23)$$

where $\mathbf{k}(n+1)$ is a gain vector, the calculation of which is detailed in [14].

The equalizer coefficient vector $\mathbf{w}(n+1)$ is then used in the passband SDFE, which has the same structure as the baseband SDFE, as shown in Fig. 5. The received passband complex signal at $t_n = n\beta T_s$ is

$$r_{iIF}(t_n) = r_i(t_n)\exp(j\omega_{IF}t_n)\big|_{t_n = n\beta T_s}, \quad (24)$$

and the feedback signal is $z_{iIF}(t_n - t_d)$. In the case of very slowly fading channel, the tap coefficient vector $\mathbf{w}(n+1)$ need not be updated for every time interval of (βT_s). The update rate depends on the channel fading rate. As we can see from the above discussion, the baseband SDFE depends on the feedback signal samples which are regenerated according to the decisions from the Viterbi decoder.

4. Performance Evaluation

The performance of the TCM schemes is studied along with that of MSK, to provide a reference. The transmitted signal bandwidth B is defined here as the 99 percent energy bandwidth: the signal power within that bandwidth is equal to 99 percent of the total signal power. For the MSK signal, $B = 1.19/T_b$, where T_b is the bit duration [15]. Therefore the spectral efficiency, R_b/B (where $R_b = 1/T_b$ is the bit rate), for MSK is 0.84 bits/s/Hz. For the same spectral efficiency, the modulation index h is 1/6 for a rate 1/2 trellis-coded four-level CPFSK signal, 2/9 for rate 2/3 trellis-coded

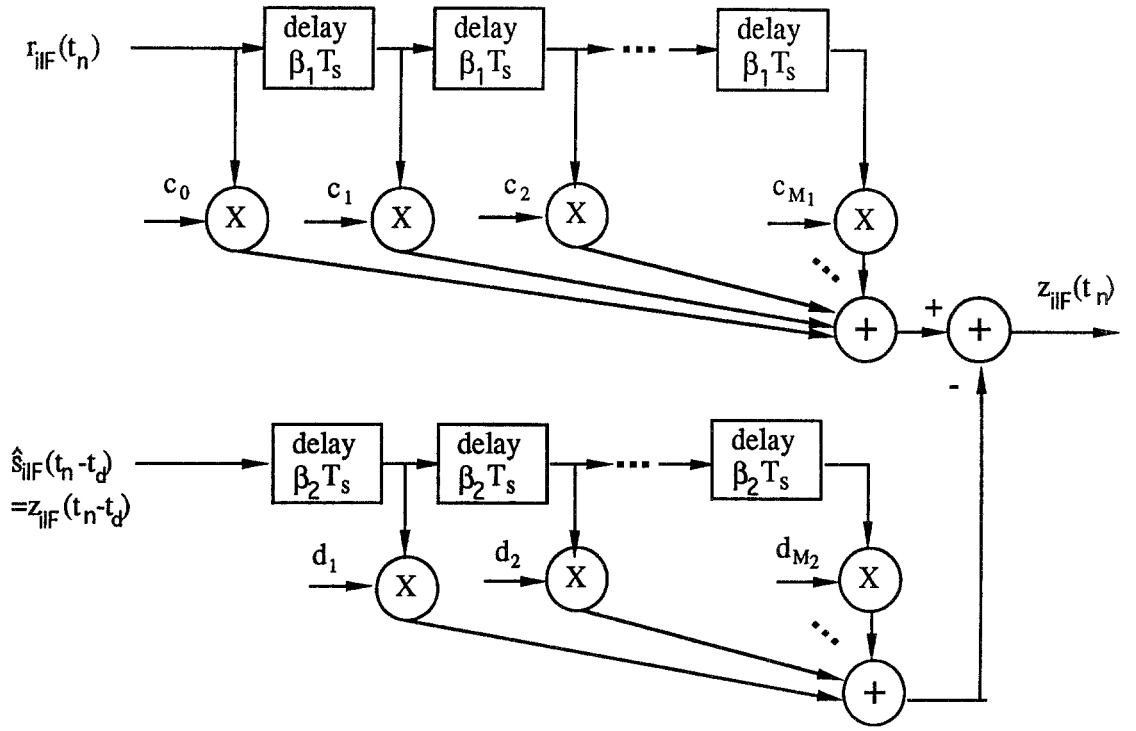

Fig. 5. Passband SDFE.

Table 2. Convolutional encodes for the investigated TCM schemes.

TCM Scheme	4-state	8-state
Rate 1/2 convolutional code with 4-level CPFSK	(7,2)	(15,2)
Rate 1/2 convolutional code with 8-level CPFSK	(7,2)	(15,4)
Rate 1/2 convolutional code with 16-level CPFSK	(5,2)	(15,2)

eight-level CPFSK, and 2/11 for rate 3/4 trellis-coded sixteen-level CPFSK. For the rate 2/3 and 3/4 TCM schemes, the trellis encoder contains a path for one or two uncoded MSB's and a rate 1/2 convolutional encoder for the remaining bit. The convolutional encoder is described by means of octal numbers for the upper and lower connection polynomials. Table 2 lists the convolutional codes for the TCM schemes to be investigated; these codes were found in [3] and [4] to be good codes for an AWGN channel and modulation indices which we used.

The performance of the TCM schemes is studied via Monte Carlo computer simulations. A system simulation model (Fig. 1) is developed within the Block Oriented Systems Simulator (BOSS) simulation package under a UNIX programming environment. The simulation results are given with 90 percent confidence intervals of (0.8 BER, 1.2 BER); the tradeoff here is computer time. The decoding depth of the Viterbi decoder is set to at least $6(K+1)$ to balance the decoder complexity and performance, where K is the constraint length of the code. The E_b/N_0 value of the received signal is defined as the ensemble average ratio of the one-bit energy of the input signals from all paths to the one-sided power spectral density of the input white Gaussian noise.

4.1. Performance Improvement by TCM

Figure 6 shows the performance of the TCM schemes in a flat Rayleigh fading channel. The performance of MSK with both noncoherent and differential detection is also given, for comparison. The fading rate $f_D T$ (= 0.005) is the same for all coded and uncoded schemes. It can be observed that noncoherent detection has a much lower error floor (especially with the TCM schemes) when compared with differentially detected MSK. Also the rate 1/2 TCM with 4 and 8 states has better performance than MSK with differential detec-

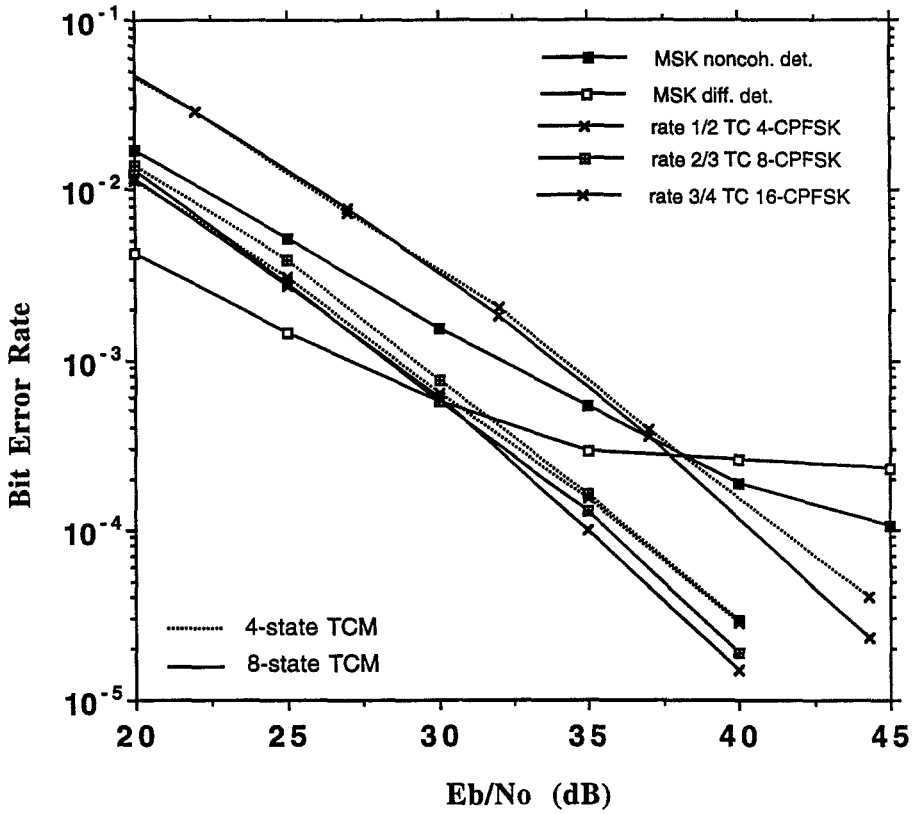

Fig. 6. BER performance of trellis coded and uncoded CPFSK schemes in a flat Rayleigh fading channel with $f_D T = 0.005$.

tion when the E_b/N_0 ratio is larger than 37.5 dB. The rate 2/3 and 3/4 TCM schemes (with 4 and 8 states) have a BER very close to each other. They outperform differentially detected MSK when the E_b/N_0 ratio is larger than (30 $\sim$ 32) dB.

Figure 7 shows the performance of the investigated modulation schemes over a six-path Rayleigh fading channel with delay spread $\sigma = 0.125T_b$ (which corresponds to 108.5 nanoseconds for the DECT system, a typical value for an indoor environment). The bit rate is the same for all schemes, with $f_D T_b = 0.005$. MSK with noncoherent detection is seen to have a lower error floor than MSK with differential detection. The 4-state TCM schemes outperform MSK with differential and noncoherent detection when the E_b/N_0 ratio is larger than (15 $\sim$ 17.5) dB, and have an error floor that is lower by more than one order of magnitude. Figure 8 illustrates the modulation performance over a six-path Rayleigh fading channel with the delay spread increased to $\sigma = 0.163T_b$ (which corresponds to 141.0 nanoseconds for the DECT system, and is a typical value for indoor to outdoor and outdoor environments). For this case, the performance improvement of the TCM schemes with noncoherent detection over MSK is significant. The error floor is also reduced by more than one order of magnitude. However, it is also observed that an increase of the delay spread corrupts the performance of all the schemes investigated. With this delay spread, even the TCM schemes cannot provide satisfactory performance (which is defined as a BER $\leq 10^{-3}$ for digital voice transmission). Diversity reception has been investigated to improve the performance of uncoded systems over a frequency-selective Rayleigh fading channel. It has been shown [8] that with the same delay spread, the performance of the DECT system is marginal even when diversity is used. Figure 9 shows the performance when the delay spread is further increased to $\sigma = 0.250T_b$ (which corresponds to 217.0 nanoseconds for the DECT system, and is the worst case for an indoor channel). Although the TCM schemes have an obvious performance improvement over MSK, the bit error rate

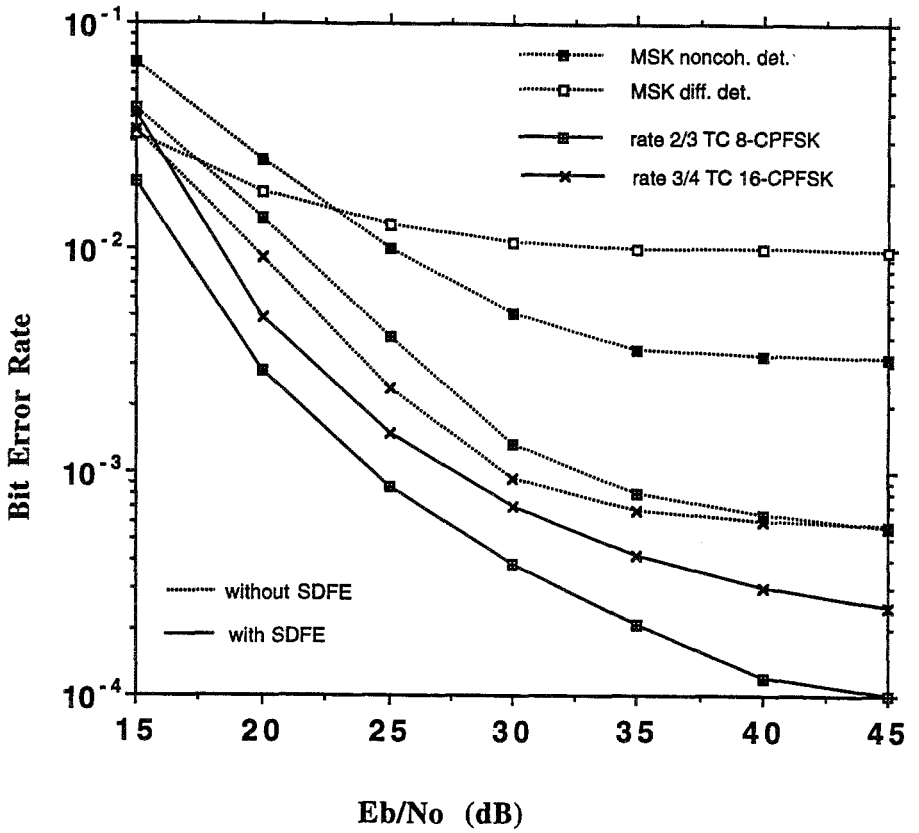

Fig. 7. BER performance in a six-path frequency-selective Rayleigh fading channel with $f_D T_b = 0.005$ and $\sigma = 0.125T_b$ (4-state TCM used).

is still unacceptable for a reliable voice transmission. With such a large delay spread, uncoded systems with diversity reception also fail to provide acceptable performance [8].

Comparing the performance in a flat Rayleigh fading channel and a frequency-selective Rayleigh fading channel with increasing delay spread, in Figs. 6–9, we observe that: (i) the TCM schemes outperform MSK in Rayleigh fading channels, especially in frequency-selective Rayleigh fading channels; (ii) With increasing delay spread, the performance of all the schemes deteriorates significantly; the error floor is increased by more than one order of magnitude when the delay spread is increased from $0.125T_b$ to $0.25T_b$; (iii) The rate 3/4 TCM scheme yields the best performance in frequency-selective fading channels; because the bit rate is the same for all the schemes investigated, the symbol duration T of the rate 3/4 TCM is 3 times that of MSK and 1.5 times that of the rate 2/3 TCM; with larger T, the value of (σ/T) is smaller, so that the effect of the delay spread σ on the BER performance degradation is reduced; (iv) In the case of large delay spread, Figs. 8–9, even the TCM schemes cannot provide an acceptable bit error rate; therefore, other channel impairment mitigation techniques (e.g. equalization) are required for better performance.

4.2. Performance Improvement by Channel Equalization

In the computer simulations, perfect post-estimation of the initial carrier phase and the ideal feedback signals at baseband and passband are assumed. A SDFE with 2-tap feed-forward transversal filter and 5-tap feedback transversal filter is implemented in the system model. $T_b/T_s = 16$ and the RLS algorithm parameter $\lambda = 0.985$ is chosen because of the slow time-varying fading channel.

The choice of the time delay t_d for the first tap in the feedback transversal filter is crucial for system performance improvements. For the case of a low E_b/N_0 environment, a large t_d should be used, because other-

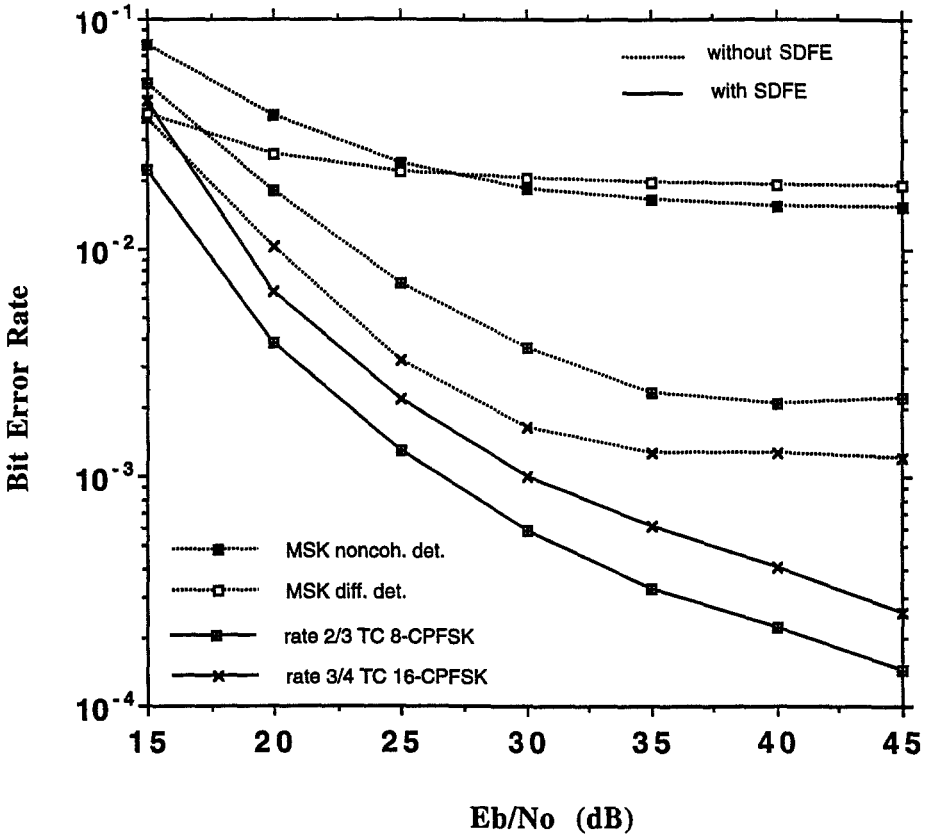

Fig. 8. BER performance in a six-path frequency-selective Rayleigh fading channel with $f_D T_b = 0.005$ and $\sigma = 0.163T_b$ (4-state TCM used).

wise the large noise component in the received signal will make the RLS algorithm pick up the feedback signal of the first tap as an equalized signal. As a result, a "false" equalization is performed since the difference between the ideal signal and the feedback signal can be much smaller than the noise component if t_d is small. On the other hand, for the case of a high E_b/N_0 environment, a small t_d should be chosen in order to effectively remove the ISI resulting from the multipath signals with small delays (less than a bit duration). Therefore, the equalizer parameter t_d should be selected adaptively according to the E_b/N_0 value of the received signal. In the following computer simulations, t_d ranges from T_b to $0.375T_b$ as the value of E_b/N_0 changes from 15 dB to 45 dB. In a conventional DFE, the value of $(t_d + \beta_2 T_s)$ is equal to T, which is larger than that of the SDFE used in the simulations.

Figures 7–9 illustrate the BER performance of the investigated modulation schems (with a 4-state trellis code) over a six-path Rayleigh fading channel with delay spreads of $0.125T_b$, $0.163T_b$ and $0.250T_b$ respectively. From the figures, we can observe that when the SDFE technique is applied to the system: (i) the performance of the TCM schemes is improved still further; (ii) the rate 2/3 TCM has better performance than the rate 3/4 TCM because it incurs more ISI to be equalized; (iii) the performance improvement by the SDFE is significant, particularly for $\sigma = 0.250T_b$ (Fig. 9), where the BER error floors are reduced by more than one order of magnitude due to the fact that the SDFE is more effective in canceling the ISI components from multipath signals with larger delays relative to the first path. ISI components with time delays less than the feedback signal delay $t_d + \beta_2 T_s$ cannot be completely removed. We have also determined that, a conventional symbol-spaced DFE using the same tap numbers and RLS algorithm with the same simulation parameters does not reduce the BER floors at all.

In practical applications, an ideal passband feedback signal is not available at the receiver. The equalized passband signal, i.e. the output of the passband SDFE, should be used, as shown in Fig. 3. This signal

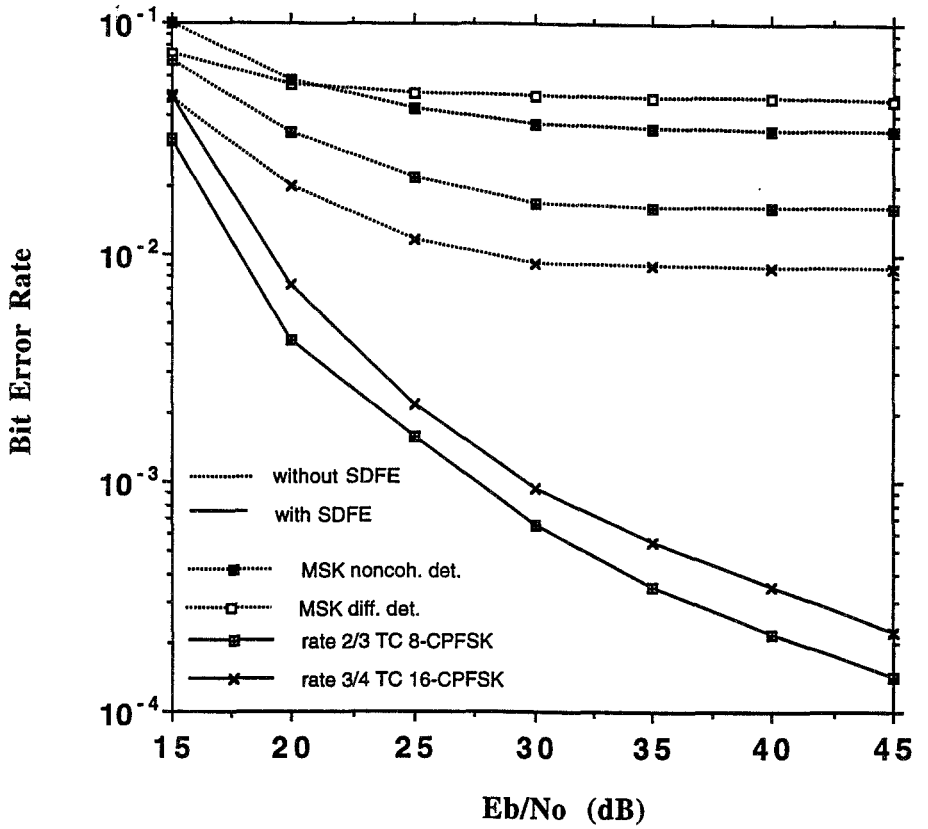

Fig. 9. BER performance in a six-path frequency-selective Rayleigh fading channel with $f_D T_b = 0.005$ and $\sigma = 0.250T_b$ (4-state TCM used).

is not regenerated from hard decisions and is not noise-free. For the case in which the first path signal experiences deep fading, the instant signal-to-noise ratio of the received first path signal at passband is dramatically reduced, which will result in a large equalization error. This problem can be solved by the use of properly designed channel precoding (transmitter-based equalization) for which an ideal and noise-free passband feedback signal is available [16].

5. Conclusions

Three trellis-coded M-ary CPFSK schemes with noncoherent detection have been studied, and their performance compared with MSK in Rayleigh fading channels. The TCM schemes with noncoherent detection significantly outperform MSK, with both differential and noncoherent detection.

A new adaptive channel equalizer has been studied in this paper for trellis-coded CPFSK schemes in an indoor wireless channel with slow fading. The soft-decision feedback equalizer can effectively mitigate channel impairments when: (i) the channel delay spread is smaller than a symbol duration; (ii) a nonlinear modulation scheme is used; and (iii) noncoherent (envelope) demodulation is used in the receiver. The results of computer simulations with ideal feedback signal samples show that the bit error rate floors of the trellis-coded CPFSK schemes are reduced by more than one order of magnitude by the equalizer. The TCM schemes combined with the equalizer can provide a satisfactory bit error rate for reliable digital voice transmission in indoor, indoor to outdoor and outdoor micro-cellular environments.

The TCM schemes with the newly proposed soft-decision feedback equalizer are especially suitable for applications where spectral efficiency, constant envelope and noncoherent detection are the preferred characteristics, such as in indoor portable and mobile communications.

References

1. GSM Recommendation Series 05, ETSI, 1990.
2. Digital European Cordless Telecommunications (DECT) – Common Interface, European Telecommunication Standard ETS-300-175, ETSI, 1992.
3. J. Anderson, T. Aulin and C.-E. Sundberg, Digital Phase Modulation, New York: Plenum Press, 1986, Chapter 11.
4. P. K. M. Ho and P. J. McLane, "Spectrum, distance, and receiver complexity of encoded continuous phase modulation", IEEE Trans. Inform. Theory, Vol. IT-34, No. 5, pp. 1021–1032, 1988.
5. K. Hirade, et al., "Error-rate performance of digital FM with differential detection in land mobile radio channels", IEEE Trans. Veh. Tech, Vol. VT-28, pp. 203–212, 1979.
6. D. L. Schilling and R. Bozovic, "On the performance of spectrally efficient trellis coded FM modulation employing noncoherent FM demodulation", IEEE J. Select. Areas Commun. Vol. 7, No, 9, pp. 1318–1327, 1989.
7. P. H. Wittke, Y. M. Lam, and M. J. Schefter, "The performance of trellis-coded nonorthogonal noncoherent FSK in noise and jamming", to appear in IEEE Trans. Commun.
8. T. A. Wilkinson, "Channel modelling and link simulation studies for the DECT test bed program", Proc. Sixth IEE Inter. Conf. on Mobile and Personal Commun., Coventry, UK, pp. 293–299, 1991.
9. H. H. Hashemi, "The indoor radio propagation channel", Proc. IEEE, Vol. 81, No. 7, pp. 943–967, 1993.
10. A. A. M. Saleh and R. A. Valenzuela, "A statistical model for indoor multipath propagation", IEEE J. Select. Areas Commun. Vol. SAT-5, No. 2, pp. 128–137, 1987.
11. W. C. Jakes (ed.), Microwave Mobile Communications, John Wiley & Sons: New York, 1974.
12. P. Monsen, "Theoretical and measured performance of DFE modem on a fading multipath channel", IEEE Trans. Commun., Vol. COM-25, pp. 1144–1153, 1977.
13. S. U. H. Qureshi, "Adaptive equalization", Proc. IEEE, Vol. 74, No. 9, pp. 1349–1387, 1985.
14. S. Haykin, Adaptive Filter Theory, 2nd edition, Prentice Hall: Englewood Cliffs, NJ, 1991, Chapter 13.
15. S. Benedetto, E. Biglieri and V. Castellani, Digital Transmission Theory, Prentice Hall Inc., Englewood Cliffs, NJ, 1987, Chapter 4.
16. W. Zhuang, W. A. Krzymien, and P. A. Goud, "Adaptive channel precoding for slowly fading channels", Proc. Fifth IEEE Inter. Symp. on Personal, Indoor and Mobile Radio Communications (PIMRC'94), Hague, The Netherlands, pp. 660–664, 1994.

Weihua Zhuang received the B.Sc. (1982) and M.Sc. (1985) degrees from Dalian Marine University (China) and the Ph.D. degree (1992) from the University of New Brunswick (Canada), all in electrical engineering. From January 1992 to September 1993, she was a Post Doctoral Fellow first at the University of Ottawa and then at Telecommunications Research Labs (TRLabs, Edmonton), working on land mobile satellite communications and indoor wireless communications. Since October 1993, she has been with the Department of Electrical and Computer Engineering, University of Waterloo, where she is an Assistant Professor. Her current resarch interests are in wireless personal communications, including digital transmission over fading channels, wireless networking, and radio positioning.

Witold A. Krzymien received his M.Sc. (Eng.) and Ph.D. degrees (both in Electrical Engineering) in 1970 and 1978, respectively, from the Poznan Technical University in Poznan, Poland. He was awarded the Minister's of Science and Technology Prize of Excellence for his Ph.D. thesis.

From 1970 to 1978 he was a Research Engineer and Teaching Assistant, and then from 1978 to 1980

an Assistant Professor of Electrical Engineering at the Poznan Technical University. In 1980 he won a Dutch Government Research Fellowship at the Twente University of Technology in Enschede, the Netherlands, for the year of 1980/1981. In the following year of 1981/82 he was a Research Assistant Professor there. From 1982 to 1986 he was an Assistant Professor of Electrical Engineering at Lakehead University in Thunder Bay, Ontario, Canada. In 1986 he joined the University of Alberta and Alberta Telecommunications Research Centre (now Telecommunications Research Laboratories, or TRLabs) as an Associate Professor of Electrical Engineering. Presently, he is a Professor of Electrical Engineering there. His current research interests are in signal processing techniques for efficient digital transmission in third-generation wireless cellular and personal communication systems employing code division or time division multiple access schemes. He spent the 1993/94 academic year as a Senior Industrial Fellow at Bell-Northern Research in Montreal, Quebec, working on effective synchronization and discontinuous transmission schemes for code division multiple access microcellular systems.

Dr Krzymien is a licenced Professional Engineer in the Province of Ontario, Canada and a Senior Member of the Institute of Electrical & Electronics Engineers (IEEE). He received the 1991/92 A. H. Reeves Premium Award in digital coding from the Institution of Electrical Engineers (U.K.) for a paper published in the *IEE Proceedings, Part I.*

Paul A. Goud received the B.Sc. degree in electrical engineering (with distinction) from the University of Alberta, Edmonton, Canada in 1959, and the M.A.Sc. and Ph.D. degrees in electrical engineering from the University of British Columbia, Vancouver, Canada in 1961 and 1964, respectively.

He was with Bell-Northern Research Ltd., Ottawa, Canada, engaged in microwave electronics research, during 1965–1966. He joined the University of Alberta in 1966, where he holds the rank of Professor of Electrical Engineering. Concurrently, he is an Adjunct Professor at the telecommunications research consortium TRLabs (since its establishment in 1985). He has also participated in microwave electronics research at AT&T-Bell Labs (USA, 1969) and Philips Research Laboraties (the Netherlands, 1973–1974). He has been the recipient of an AGT Professorship, a McCalla Research Professorship and a NSERC Industrial Research Fellowship. His current research interests include topics in mobile communications, namely coded modulation, RF power amplifier linearization and integrated RF/DSP design.

Dr Goud is a Senior Member of the IEEE and a registered Professional Engineer.